RSC Advances

Design, synthesis, and docking studies of some novel isocoumarine analogues as antimicrobial agents

Journal:	*RSC Advances*
Manuscript ID:	RA-ART-07-2014-007223.R1
Article Type:	Paper
Date Submitted by the Author:	06-Sep-2014

Complete List of Authors:	ashraf, muhammad; AIOU, chemistry; kungju national university, biology Saeed, Aamer; Quaid-I-Azam University 45320 Islamabad, Chemistry nadeem, humaira; Riphah Institute of Pharmaceutical Sciences, Riphah International University, chemistry

The isocoumarins have been designed and prepared by incorporating the NSAIDs to discover potential inhibitors of UDP-N-acetylmuramyl-L-alanine ligase (MurC)

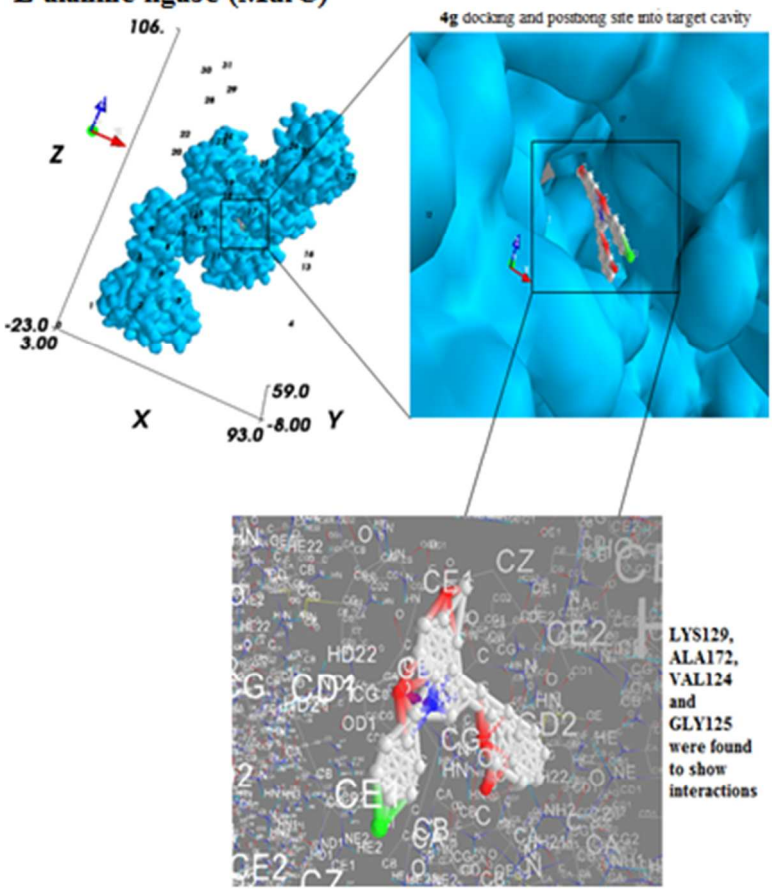

Design, synthesis and docking studies of some novel isocoumarin analogues as antimicrobial agents

Zaman Ashraf [a,b*], Aamer Saeed[c] and Humaira Nadeem [d]

[a] *Department of Chemistry, Allama Iqbal Open University, Islamabad 44000, Pakistan.*

[b]*Department of Biology, College of Natural Sciences, Kongju National University, Kongju 314-701, south Korea.*

[c]*Department of Chemistry, Quaid-I-Azam University, Islamabad 45320, Pakistan.*

[d]*Riphah Institute of Pharmaceutical Sciences, Riphah International University, Islamabad, 44000, Pakistan*

*** Address for Correspondence**

Dr. Muhammad Zaman Ashraf

Chemistry Department, Allama Iqbal Open University, Islamabad, Pakistan.

Email: mzchem@yahoo.com

Contact number: 0092 3215194461, 00929057182

Fax: 0092512891471

Abstract

A number of novel isocoumarin analogues have been synthesized by condensation of homophthalic acid anhydride with different non-steroidal anti-inflammatory drugs (NSAIDs). To investigate the antimicrobial data on structural basis, *in-silico* docking studies of the synthesized compounds **(4a-4g)** into the crystal structure of UDP-N-acetylmuramate-L-alanine ligase using Autodock PyRx virtual screening program was performed in order to predict the affinity and orientation of the synthesized compounds at the activities. UDP-N-acetylmuramate-L-alanine ligase is essential for d-glutamate metabolism and peptidoglycan biosynthesis in bacteria. R2 values showed good agreement with predicted binding affinities obtained by molecular docking studies. The results indicate that the basic nucleus portion of the **(4c)**, **(4g)**, **(4f)** and **(4a)** binds into the specificity pocket. In this pocket the Isocoumarin nucleus of these compounds interact with amino acid residue of the target. Also, it is verified by *in vitro* antimicrobial screening, where all the compounds were active against tested bacterial strains. Among these compounds **(4c)**, **(4g)**, **(4f)** and **(4a)** showed good bacterial zone inhibition.

Keywords: Isocoumarins; *In vitro* Antimicrobial activity; Molecular docking

Introduction

Isocoumarins and 3,4-Dihydroisocoumarins (3,4-dihydro-*1H*-2-benzopyran-ones) are natural lactones, isolated from a wide range of natural sources (microbes, plant and insects) and encompass an array of biological activities including nephrotoxic, hepatotoxic, cytotoxic, immunomodulatory, algicidal, gastroprotective, protease inhibition, antifungal and antimalarial activities.[1–6] They also display anti-inflammatory, antiangiogenic and antiallergic activities.[7-9] Isocoumarins are also used as a lead compound for the identification of insecticides which selectively bind at the insect GABA receptor.[10]

3-Substituted isocoumarins also exhibit anti HIV activity *in vitro*, diuretic, antihypertensive, antiarrythmics, β-sympatholytics, anticorrosive, laxatives, asthmolytic, phytotoxic and are useful in the treatment of emphysema.[11] Isocoumarin derivatives are potential inhibitors of endothelial cell proliferation, migration, sprouting, tube formation *in vitro*, and tumor growth *in vivo*.[12]

Molecular docking plays an important role in the rational design of drugs. In the field of molecular modeling, docking is a method which predicts the preferred orientation of one molecule to a second when bound to each other to form a stable complex. Molecular docking can be defined as an optimization problem which would describe the ‘‘best-fit’’ orientation of a ligand that binds to a particular protein of interest.[13,14] 3-substituted isocoumarins exhibited valuable pharmacological activities. Therefore, on continuation of our work[15-17] efforts have been directed towards the synthesis of new isocoumarins analogues as excellent antimicrobial agents.

Peptidoglycans are the main constituents of the bacterial cell wall which imparts the structural strength to the bacterial cell wall and perform different functions as it counteracts the osmotic pressure of the cytoplasm. UDP-N-acetylmuramate-L-alanine ligase also named shortly (MurC synthetase) is essential and unique enzyme participates in d-glutamine and d-glutamate metabolism and intracellular pathway of bacterial peptidoglycan biosynthesis.[18] The MurC synthetase with D-alanine-D-alanine ligase (EC 6.3.2.4), UDP-N-acetylmuramoyl-L-alanyl-D-glutamate-L-lysine ligase (EC 6.3.2.7) or UDP-N-acetylmuramoyl-L-alanyl-D-glutamate-2,6-diaminopimelate ligase (EC 6.3.2.13), UDP-N-acetylmuramoyl-L-alanine-D-glutamate ligase

(EC 6.3.2.9) and UDP-N-acetylmuramoyl-tripeptide-D-alanyl-D-alanine ligase (EC 6.3.2.10) involved in the synthesis of bacterial cell-wall peptide. In 2004, Ehmann et al. reported that UDP-N-acetylmuramyl-L-alanine ligase (MurC) is an important target for the discovery of novel antibacterial agents as it involved in peptidoglycan biosynthesis.[19]

In this paper, we report the design, synthesis, antimicrobial activity and docking studies of novel isocoumarin derivatives, planned as UDP-N-acetylmuramyl-L-alanine ligase (MurC) inhibitors candidates. The synthesis of the final compounds was accomplished by using the bases N,N,N',N'-tetramethylguanidine (TMG) and triethylamine with high yield. *In-silico* docking studies of the synthesized compounds into the crystal structure of MurC synthetase were performed using Autodock PyRx virtual screening program. The synthesized compounds were then tested against ten different gram positive and gram negative bacteria.

Experimental

Melting points were recorded using a digital Gallenkamp (SANYO) model MPD BM 3.5 apparatus and are uncorrected. ^{1}H NMR and the ^{13}C NMR spectra were determined as $CDCl_3$ solutions at 300 MHz and 100 MHz respectively, on a Bruker AM-300 machine. FTIR spectra were recorded using an FTS 3000 MX spectrophotometer; Mass Spectra (EI, 70eV) on a GC-MS instrument and elemental analyses with a LECO-183 CHNS analyzer. The analytical TLC was carried out using recoated plated from Merck and thick layer chromatography using silica gel from Merck.

Synthesis of homophthalic acid anhydride (1)

A solution of homophthalic acid (2.0g, 12.34 mmol) in dry toluene (35 mL) was treated with acetic anhydride (1.1g, 10mL, 10.8 mmol). The reaction mixture was refluxed for 1 hr and then poured into ice cold water. The organic layer was separated, dried over anhydrous sodium sulfate and toluene was rotary evaporated to get homophthalic acid anhydride **(1).** Yield 82%; R_f: 0.7 (petroleum ether and ethyl acetate, 4:1); m. p. 140-142°C; IR (KBr): 3011 (C-H), 1735 (C=O), 1590 (C=C) cm^{-1}; ^{1}H NMR ($CDCl_3$, δ ppm): 7.85 (1H, d, *J*=3.7, H-8), 7.3-7.4 (2H, m, H-6, H-7), 6.97 (1H, d, *J*=3.4, H-5), 3.47 (2H, s, H-4); ^{13}C NMR ($CDCl_3$, δ ppm): 165.5 (C3), 147.1 (C1), 137.2 (C4a), 134.4 (C6), 131.5 (C8a), 130.7 (C8), 129.7 (C5), 127.5 (C7), 38.2 (C4);

MS (70eV): m/*z* (%) ; 162 [M^+] (25), 134 (43), 118 (100), 90 (32); Anal. Calcd. for $C_9H_6O_3$: C, 66.66 H, 3.70; Found: C, 66.53 H, 3.59.

General procedure for 3-alkyl/arylisocoumarins (4a-g)

A mixture of aliphatic/aromatic carboxylic acids **(2a-j)** (1 mmol) and thionyl chloride (1.2 mmol) was refluxed for 1 hr in the presence of a drop of DMF. The completion of reaction was determined by stoppage of evolution of gas. Excess of the thionyl chloride was rotary evaporated to afford acid chlorides **(3a-j)**.

A solution of homophthalic acid anhydride **(1)** (2.00 mmol) in acetonitril (12mL) was added to a solution of N,N,N',N'-tetramethylguanidine (TMG) (2.20 mmol) in acetonitril (5mL) over 36 min maintaining an internal temperature of 0°C. Triethylmine (4.0 mmol) was added in one portion. Acid chlorides **(3a-j)** (3.20 mmol) were added over 3 min and the mixture was stirred for an additional 20 min. After the completion of reaction the cooling bath was removed and reaction was allowed to warm to room temperature. The reaction mixture was quenched by the addition of HCl (1M, 5mL). The two phases were separated and organic layer was washed with saturated sodium chloride solution and then dried (Na_2SO_4) prior to removal of solvent under reduced pressure to dryness. Isocoumarins **(4a-j)** were then purified by preparative thin layer chromatography using (petroleum ether and ethyl acetate, 7:3) as eluant.

3-[(*S*)-1'-(4''-isobutylphenyl)ethyl)]isocoumarin (4a)

Yield 75%; Light yellow oil; IR (neat): υ =1710, 1597, 1506 cm^{-1}; ^1H NMR ($CDCl_3$): δ 0.89 (6H, d, *J*=6.6 Hz, $2CH_3$ of isobutyl), 1.64 (3H, d, *J*=7.2 Hz, H-2'), 1.85 (1H, m, CH of isobutyl), 2.45 (2H, d, *J*=7.1 Hz, CH_2 of isobutyl), 3.92 (1H, q, *J*=7.2 Hz, H-1'), 6.25 (1H, s, H-4), 7.10 (2H, d, *J*=8.1 Hz, H-3'',H-5''), 7.23 (2H; d, *J*=8.1 Hz, H-2'', H-6''), 7.33 (1H, d, *J*=7.9 Hz, H-5), 7.43 (1H, dt, *J*=8.1, 1.0 Hz, H-7), 7.64 (1H, dt, *J*=7.8, 1.3 Hz, H-6), 8.23 (1H, d, *J*=7.7 Hz, H-8); EIMS: m/z (%) =306 (100) [M^+], 264 (53.2), 263 (88.2), 249 (57.1), 235 (23.3), 189 (7.4), 161 (27.5), 145 (94.1), 119 (23.2), 117 (78.2), 89 (92.9); HRMS: 306.1625 (calcd for $C_{21}H_{22}O_2$, 306.1620).

3-[1'-(3''-Fluoro-4''-biphenyl)ethyl]isocoumarin (4b)

Yield 68%; Light yellow oil; IR (neat): υ =1723, 1647, 1617, 1580 cm^{-1}; ^1H NMR ($CDCl_3$): δ 1.27 (3H, d, *J*=7.5 Hz, CH_3), 3.69 (1H, q, *J*=7.5 Hz, H-1'), 6.70 (1H, s, H-4), 6.93 (2H, m, H-2', 6'), 7.1 (1H, d, *J*=8.1 Hz, H-4''), 7.30–7.41 (5H, m, H-5', 2'', 3'', 5'', 6''), 7.49 (1H, dt, *J*=7.6, 1.2 Hz, H-7), 7.55 (2H, m, H-5, H-6), 8.10 (1H, d, *J*=7.6 Hz, H-8); EIMS: m/z (%) =344 (15.4) [M^+], 329 (15.2), 325 (2.6), 301 (10.2), 267 (7.1), 227 (5.1), 199 (100), 173 (5.3), 171 (7.5), 155 (9.5), 145 (20.1), 117 (9.8), 89 (26.2); HRMS: 344.1221 (calcd for $C_{23}H_{17}FO_2$, 344.1213).

3-[1'-(5''-Methoxy-2''-naphthyl)ethyl]isocoumarin (4c)

Yield 62%; m.p. 35°C; IR (KBr): υ=1705 (C=O, lactonic), 1645, 1601, 1498 cm^{-1}; ^1H NMR ($CDCl_3$): δ 1.57 (3H, d, *J*=7.2 Hz, CH_3), 3.90 (3H, s, OCH_3), 4.13 (1H, q, *J*=7.2 Hz, H-1'), 6.75 (1H, s, H-4), 6.81–6.89 (2H, m, H-5', H-7'), 6.95–7.18 (4H, m, H-1', 3', 4', 8'), 7.24 (1H, d, *J*=7.5 Hz, H-5), 7.34 (1H, dd, *J*=7.4, 1.3 Hz, H-7), 7.41 (1H, dd, *J*=7.3, 1.9 Hz, H-6), 8.01 (1H, d, *J*=7.6 Hz, H-8); EIMS: m/z (%) =330 (8.4) [M^+], 300 (37.1), 213 (6.5), 185 (100), 173 (15.5), 157 (17.2), 155 (17.8), 145 (5.9), 117 (9.8), 89 (26.2); HRMS: 330.1245 (calcd $C_{22}H_{18}O_3$, 330.1256).

3-[1'-(4''-Isobutylphenyl)ethyl]isocoumarin (4d)

Yield 65%; Light yellow oil; IR (neat): υ =1710, 1597, 1506 cm^{-1}; ^1H NMR ($CDCl_3$): δ 0.89 (6H, d, *J*=6.6 Hz, $2CH_3$ of isobutyl), 1.64 (3H, d, *J*=7.2 Hz, H-2'), 1.85 (1H, m, CH of isobutyl), 2.45 (2H, d, *J*=7.1 Hz, CH_2 of isobutyl), 3.92 (1H, q, *J*=7.2 Hz, H-1'), 6.25 (1H, s, H-4), 7.10 (2H, d, *J*=8.1 Hz, H-3'',H-5''), 7.23 (2H; d, *J*=8.1 Hz, H-2'', H-6''), 7.33 (1H, d, *J*=7.9 Hz, H-5), 7.43 (1H, dt, *J*=8.1, 1.0 Hz, H-7), 7.64 (1H, dt, *J*=7.8, 1.3 Hz, H-6), 8.23 (1H, d, *J*=7.7 Hz, H-8); EIMS: m/z (%) =306 (100) [M^+], 264 (53.2), 263 (88.2), 249 (57.1), 235 (23.3), 189 (7.4), 161 (27.5), 145 (94.1), 119 (23.2), 117 (78.2), 89 (92.9); HRMS: 306.1625 (calcd for $C_{21}H_{22}O_2$, 306.1620).

3-[2'-(2'',6''-dichlorophenylamino)benzyl]isocoumarin (4e)

Yield 65%; m.p. 52 °C; IR (KBr): υ =3421, 1719, 1607, 1523 cm^{-1}; ^1H NMR ($CDCl_3$): δ 2.09 (2H, s, CH_2), 4.52 (1H, s, -NH), 6.35 (1H, s, H-4), 6.41 (1H, d, *J*=6.5 Hz, H-3'), 6.5-6.7 (3H, m, H-4'-H-6'), 6.81 (1H, dd, *J*=7.2, 6.8 Hz, H-4''), 7.95 (2H, d, *J*=7.8 Hz, H-3'', H-5''), 7.13 (1H; d, *J*=8.1 Hz, H-5), 7.3-7.4 (2H, m, H-6, H-7), 7.43 (1H, d, *J*=7.4 Hz, H-8); EIMS: m/z (%) =396

(100) [M^+], 265 (44.5), 251 (33.2), 235 (23.3), 189 (7.4), 161 (27.5), 145 (82.1), 119 (19.2), 117 (78.2), 89 (92.9). HRMS: 396.2678 (calcd for $C_{22}H_{15}Cl_2NO_2$, 396.2669).

3-[2'-(2'',3''-dimethylphenylamino)phenyl]isocoumarin (4f)

Yield 73%; m.p. 45 °C; IR (KBr): υ =3354, 1731, 1586, 1503 cm^{-1}; ^1H NMR ($CDCl_3$): δ 2.27 (3H, s, CH_3), 2.34 (3H, s, CH_3), 4.52 (1H, s, -NH), 6.41 (1H, s, H-4), 6.5-6.6 (3H, m, H-4''-H-6''), 6.65 (1H, d, *J*=7.2 Hz, H-3'), 6.7-6.9 (3H, m, H-4'-H-6'), 7.15 (1H, d, *J*=6.5 Hz, H-5), 7.3-7.5(2H, m, H-6, H-7), 7.63 (1H, d, *J*=6.2 Hz, H-8); EIMS: m/z (%) =341 (100) [M^+], 265 (44.5), 251 (33.2), 235 (23.3), 145 (74.5), 119 (25.2), 117 (81.6), 89 (76.8). HRMS: 341.4024 (calcd for $C_{23}H_{19}NO_2$, 341.4036).

3-[(1'-(4'''-chlorophenyl)-5''-methoxy-2''-methyl-1*H*-indol-3''-yl)methyl]isocoumarin (4g)

Yield 53%; m.p. 140 °C; IR (KBr): υ =1725, 1645, 1573, 1503 cm^{-1}; ^1H NMR ($CDCl_3$): δ 2.31 (3H, s, CH_3), 2.76 (2H, s, CH_2), 3.85 (3H, s, OCH_3), 6.25 (1H, s, H-4''), 6.45 (1H, s, H-4), 6.5-6.6 (2H, m, H-6''-H-7''), 7.15 (1H, d, *J*=7.7 Hz, H-5), 7.3-7.5(2H, m, H-6, H-7), 7.65 (2H, d, *J*=8.5 Hz, H-3''', H-5'''), 7.71 (2H, d, *J*=6.3 Hz, H-2''', H-6'''), 7.78 (1H, d, *J*=7.6 Hz, H-8); EIMS: m/z (%) =460 (25) [M+2], 458 (100) [M^+], 265 (34.2), 145 (62.5), 119 (21.1), 117 (92.2), 89 (54.4). HRMS: 457.9050 (calcd for $C_{27}H_{20}ClNO_4$, 457.9062).

Antibacterial activity

In vitro evaluation of antibacterial activity of the 3-substituted isocoumarins **(4a-g)** was carried out by agar well diffusion assay against ten different Gram positive and Gram negative bacteria. The seven were Gram negative *viz. Proteus mirabilis* (ATCC 49565)*, Escherichia coli* (ATCC 25922)*, Pseudomonas aeruginosa* (ATCC 33347)*, Pseudomonas putida* (ATCC 47054)*, Salmonalla typhi* (ATCC 19430)*, Shigella flexineri* (ATCC 25929) and *Klebsiella pneumoniae* (ATCC 43816) and three were Gram positive *viz Bacillus subtilis* (ATCC 6633), *Staphylococcus aureus* (ATCC 29213) and *Micrococcus luteus* (ATCC 9341).[20] Antibacterial activity was determined by using the Mueller Hinton Agar (MHA). The fresh inoculums of these bacteria were prepared and diluted by sterilized normal saline. The turbidity of these cultures was adjusted by using 0.5Mc-Farland. A homogeneous bacterial lawn was developed by sterile cotton swabs. The inoculated plates were bored by 6 mm sized borer to make the wells. The sample

dilutions were prepared by dissolving each sample (1.0mg) in 1.0 mL of DMSO used as negative control in this bioassay. The equimolar concentration of Levofloxacin (1.0mg/ml), a broad spectrum antibiotic (positive control) was prepared. These plates were incubated at 37 °C for 24 hours. Antibacterial activity of these three series of compounds was determined by measuring the diameter of zone of inhibition (mm, ± standard deviation) and presented by subtracting the activity of the negative control Table 1.

Docking studies

Preparation of the ligands

MOL SDF format of all ligands were prepared and was further translated to PDBQT file using PyRx virtual screening tool to generate 3D atomic coordinates of a molecule. Discovery Studio 3.0 visualizer was used to label the atoms of the molecule. Finally these ligands models were evaluated for docking procedure. The AutoGrid dimensions between ligands and enzyme are: Grid Center X: 48.6290, Y: 23.4707, Z: 43.7046 with total number of points X: 50, Y: 50, Z: 50 and Spacing (Angstrom): 0.3750. The compounds were then tested for Lipinski's Rule of 5 using the Molinspiration server (http://www.molinspiration.com). Table 2 presented the structural properties of the isocoumarin derivatives **(4a-g)**.

Accession of the target protein

The crystallographic 3D structure of UDP-N-acetylmuramate—L-alanine ligase was accessed from Protein Data Bank (PDB ID: 1GQQ). The resolution of the XRD structure of this model enzyme is 3.10A° with R-value of 0.241 (obs.). The length (Å) and angles (°) properties of the structure respectively are: a=65.51, b=99.49, c=180.59 and α=90.00, β=90.00, γ=90.00. The active site was defined from the coordinates of the ligand in the original target protein sites. The active recognition site of the ensemble has been defined as the collection of residues within 25.0 Å of the bound inhibitor and comprised the union of all ligands of the ensemble. All atoms located less than 25.0 Å from any ligand atom were identified and were considered as active site residues. The amino acid residues on MurC synthetase with shaded receptor binidng cavity defined by using Discovery Studio 3.0 Visualizer (PDB ID: 1GQQ) Analysis of Protein Model and AutoGrid of target protein exhibiting active ligand binding sites by using AutoDock Vina are shown in figure 1.

Next, biopolymer protein analysis tool was used, in a stepwise process of analysis and correction of geometry parameters. For each structure, the description of an ensemble contains the definition of the protein atoms, the resolution of ambiguities in the PDF file, the location of hydrogen atoms at hetero atoms, and the definition of the active site atoms. The assignment of hydrogen positions has been made on the basis of default rules except for the definition of the hydrogen positions inside the histidine side-chain. Water molecules contained in the PDF file have been removed. Hydrophobicity plot of MurC synthetase generated by using Discovery Studio 3.0 Visualizer. The Ramachandran Plot indicates low energy conformations for φ (phi) and ψ (psi), providing the graphical representation of the local backbone conformation of each residue of our target protein (figure 2). Points on Plot are representing the φ and ψ torsion angles of a residue. It is also representing the favorable and unfavorable regions for residues.

Lipinski's rule of five

Lipinski's rule of five was applied to evaluate in vivo absorption capabilities of the designed molecules. Any of the newly synthesized compound if satisfy the rule of five have good absorption when administered orally. A molecule have molecular mass less than 500, hydrogen bond donors (-OH, NH) less than five, hydrogen bond acceptors (N, O) less than ten and calculated log*P* is less than five satisfy the rule of five. This principle has been extensively employed on newly synthesized compounds for their further use as drug candidates. The results of the calculations for the molecules designed in this study show that all molecules have a potential for good in vivo absorption except for **(4b)** and **(4e)**. The log*P* values of compounds **(4b)** and **(4e)** are 5.88 and 7.22 respectively which are beyuond the limits of partition coeffecient.

Docking Run

In order to understand the structural basis of UDP-N-acetylmuramate-L-alanine ligase specificity, structural complexes of this target enzyme with probable synthetic inhibitors are determined using a computational docking approach. The AutoDock (PyRx) suite of programs is used to determine the binding modes of the synthetic inhibitors. Binding sites and docking run of target protein with ligand was analyzed by using the PyRx, AutoDock Vina option based on scoring functions. An exhaustive Search was performed by enabling "Run AutoGrid" option and

then "Run AutoDock" option in control panel by selecting the Lamarckian GA docking algorithm. In this approach, the ligand performs a random walk around the static protein. The energy of interaction of this single atom with the protein is assigned to the grid point. Interaction energies are calculated with a free-energy based expression comprising terms for dispersion/repulsion energy, directional hydrogen bonding. At each step of the simulation, the energy of interaction of ligand and protein is evaluated using atomic affinity potentials computed on a grid. The receptor coordinates (maximum and minimum) fit within the following volume: 90.031, 55.286, 102.112 and 8.870, -3.517, -18.845 respectively. The A and OA are the ligands atom types docked and involved in interaction with A C NA OA N SA HD target atom types.

Results and discussion

The aforementioned compounds **(4a-g)** were obtained according to the synthetic route showed in scheme 1. Homophthalic acid was treated with acetic anhydride to afford its anhydride **(1)**. The acid chlorides of different non-steroidal anti-inflammatory drugs (NSAIDs) **(3a-g)** were synthesized by reacting them with thionyl chloride in the presence of dry benzene as solvent. These acid chlorides were then condensed with homophthalic acid anhydride **(1)** yielded the target isocoumarins **(4a-g)** in good yield. The ^{1}H NMR spectra of these isocoumarins showed a characteristic signal for H-4 proton as singlet in the region between 6.3-6.8ppm. The mass spectral results also confirmed the formation of final compounds.

The *in vitro* antibacterial activity of synthesized compounds was performed against ten different Gram positive and Gram negative bacteria to evaluate their potential against these strains. All of the selected bacterial strains in this study are pathogenic. The antibacterial results show that all of the synthesized compounds afforded antibacterial activity with the greatest inhibition of bacterial growth produced by compounds **(4c)**, **(4g)**, **(4f)** and **(4a)**. The preliminary findings suggested that derivative **(4c)** exhibited more potential against Gram negative than Gram positive bacteria. The basic nucleus of isocoumarin remains the same in all of the derivatives but they differ as they have different steric bulk of the substituent present at position 3. This is the factor due to which these compounds have different hydrophobicity and absorption.

The derivative **(4c)** have methoxy substituted nephthyl moiety at position 3 of isocoumarin nucleus which selectively target Gram negative bacteria. The nephthyl group in this

case increases the hydrophobic character of the isocoumrin **(4c)** which may also determine its greater potential against Gram negative bacteria. The compound **(4g)** displayed excellent antibacterial activity compared to all other derivatives. It possess N-substituted indole scaffold which play very important role in bacterial growth inhibition. Further studies of these derivatives are required which enables us for the use of these compounds as therapeutic agents.

In an attempt to theoretically explain the difference found in the antibacterial activity of the isocoumarins **(4a-g)**, docking studies using the enzyme MurC synthetase were performed. The molecular construction and the docking analysis of isocoumarins were accomplished as described in subsequent section. Lipinski's rule of 5 also verified drug likeness properties of the compounds **(4c)**, **(4g)**, **(4f)** and **(4a)** because their logP values are below 5 while compounds **(4b)**, **(4e)** and **(4d)** have logP values beyond Partition coefficient limits. The protein-ligand interaction score values were simultaneously obtained by using the PyRx AutoDock Vina and AutoGrid option, the binding active sites and docked poses obtained were visualized and have been shown in the figures (3-9).

These inhibitors were docked with MurC synthetase using our AutoDock procedure. All the computationally predicted lowest energy complexes of MurC are stabilized by intermolecular hydrogen bonds and stacking interactions. In these computed complexes of MurC, the specificity pocket residues LEU182, PHE181, GLY125, THR131, ASN193, PHE327, GLU195, ASP345, LYS129, ALA172, VAL124, MET194, ASN193, LEU111, THR133 and THR148, ILU114, GLU113, ARG107, MET209, LYS215, VAL412, LYS208, PHE117, GLU113, ALA174, and ASP170 of MurC is involved in hydrogen bonding with the bound inhibitors.

The interactions in these complexes vary depending on the size, linkage and the functional groups. These stacking interactions have been proposed as the reason for the increased binding affinities of these larger inhibitors.

Figures (5-11) show the most energetically favorable binding mode of isocoumarins **(4a-g)** to MurC. From these figures it can be seen that the basic nucleus portion of the **(4c)**, **(4g)**, **(4f)** and **(4a)** binds into the specificity pocket. In this pocket the Isocoumarine nucleus of these compounds interacts with LEU182, PHE181, GLY125, and THR131; LYS129, ALA172, VAL124, and GLY125; MET194, ASN193, LEU111, and THR133; and MET209, LYS215,

VAL412, and LYS208 respectively amino acids residues of MurC target, while the rest of the compound showed poor absorption ability.

Analysis of different choices for combining structures into a single representative energy grid was performed in our study. These inhibitors were docked into the generated combined grids using AutoDock Vina (PyRx tool) and the RMSD from native pose and their binding energies evaluated to find that the weighed averaged grids performed greater. Table 2 presented the AutoGrid Calculation around 8043 receptor atoms of UDP-N-acetylmuramate-L-alanine ligase with minimum and maximum interacting energies. The RMSD values (Total run=9) has been discussed under Table 3.

The binding energies of the ligand target complexes during docking were calculated and presented in table 4. The higher value depicted the stable complex formed between the drug and macromolecule. The value of binding energy of derivative **(4g)** calculated during docking studies was **-**12.26 while binding energies of other derivatives **(4a)**, **(4c)** and **(4f)** were -10.33, -10.05 and -10.63 respectively. These values verified that most stable drug receptor complex was formed by compound **(4g)** with target protein. The isocoumarin nucleus with nitrogen substituted indole moiety in compound **(4g)** interacts with the LYS129, ALA172, VAL124 and GLY125 amino acids residues of the target protein. The docking results also support our findings.

Conclusion

Isocoumarin derivatives bearing non-steroidal anti-inflammatory drugs (NSAIDs) moiety have been synthesized by condensation of homophthalic acid anhydride. The synthesized compounds **(4a-g)** were evaluated for their *in vitro* antibacterial activity and *in-silico* docking studies into the crystal structure of UDP-N-acetylmuramate-L-alanine ligase using Autodock PyRx virtual screening program. In the whole series the compounds **(4c)**, **(4g)**, **(4f)** and **(4a)** showed excellent bacterial growth inhibition. The docking studies also verified that these compounds possess high affinity for the receptor and bind into the specific pocket. R2 values showed good agreement with predicted binding affinities obtained by molecular docking studies.

References

1. W. Zhang, K. Krohn, S. Draeger and B. Schulz, *J. Nat. Prod.,* 2008, **71**, 1078-1081.
2. K. F. Devienne, G. Raddi, R. G. Coelho and W. Vilegas, *J. Phytother. Phytopharm.,* 2005, **12**, 378-381.
3. L. C. DiStasi, D. Camuesco, A. Nieto, W. Vilegas, A. Zarzuelo and J. Galvez, *Planta Med.*, 2004, **70**, 315-320.
4. I. Kostova, *Curr. Med.Chem.,* 2005, **5**, 29-46.
5. K. Krohn, U. Florke, M. S. Rao, K. Steingrover, H. J. Aust, S. Draeger and B. Schulz, *Nat. Prod. Lett.,* 2001, **15**, 353-361.
6. Y. F. Huang, L. H. Li, L. Tian, L. Qiao, H. M. Hua and Y. H. Pei, *J. Antibiot.,* 2006, **59**, 355-357.
7. N. Koohei, Y. Mikikio, T. Yoshiko, K. Kenichi and N. Shoichi, *Chem. Pharm. Bull.,* 1981, **29**, 2689-2691.
8. F. Takuya, F. Yoshiyasu and A. Yoshinori, *Phytochem.,* 1986, **25**, 517-520.
9. H. L. Jeong, J. P. Yun, S. K. Hang, S. H. Young, K. Kyu-Won and J. L. Jung, *J. Antibiot.,* 2001, **54**, 463-466.
10. Y. Ozoe, T. Kuriyama, Y. Tachibana, K. Harimaya, N. Takahashi, T. Yaguchi, E. Suzuki, K. Imamura and K. Oyama, *J. Pestic. Sci.,* 2004, **29**, 328.
11. J. B. Hudson, E. A. Graham, L. Harris and M. J. Ashwood-Smith, *Phytochem. Photobiol.,* 1993, **57**, 491-496.
12. L. R. Corinne, A. Naoki, G. T. Jennifer, B. Michael, M. D. William, D. K. George, L. R. Susan, M. Michael, F. Robert, K. Raghu, K. Donald and K. Surender, *Cancer Res.,* 2002, **62**, 789-795.
13. I. A. Hamed, T. Keiichiro, A. Eiichi, K. Hiroto, M. Shinji, H. Hiroyuki, A. Noriyuki, K. Yutaka and Y. Takehiro, *Bioorg. Med. Chem.,* 2007, **15**, 242-256.

14. G. M. Maria, Z. Daniele, V. Luciano, F. Maurizio, F. Marco, P. Sabrina, S. Giuditta and B. Elena, *Bioorg. Med. Chem.,* 2005, **13**, 3797-3800.

15. S. Aamer and A. Zaman, *J. Heterocyclic Chem.,* 2008, **45**, 679-682.

16. S. Aamer, A. Zaman and R. Humaira, *J. of Asian Nat. Prod. Res.,* 2011, **13**, 97-104.

17. S. Aamer and A. Zaman, *Chem. Heterocyc. Compd.,* 2008, **44**, 967-972.

18. J. Humljan, S. Starcević, V. Car, A. P. Stefanic, D. Kocjan, B. Jenko and U. Urleb, *Pharmazie.,* 2008, **63**, 102-106.

19. D. E. Ehmann, J. E. Demeritt, K. G. Hull and S. L. Fisher, *Biochim. Biophys. Acta.,* 2004**,** **1698**, 167-174.

20. A. Zaman, M. Aun, I. Muhammad and H. T. Ahmad, *Int. J. Org. Chem.,* 2001, **1**, 257-261.

Figure 1 Amino acid residues on UDP-N-acetylmuramate-L-alanine ligase with shaded receptor binidng cavity defined by using Discovery Studio 3.0 Visualizer (PDB ID: 1GQQ)

Figure 2 The Ramachandran Plot indicates low energy conformations for φ (phi) and ψ (psi), providing the graphical representation of the local backbone conformation of each residue of our target protein. Points on Plot are representing the φ and ψ torsion angles of a residue. It is also representing the favorable and unfavorable regions for residues.

Figure 3 Complexity of protein–ligand interactions. The figure shows a schematic illustration of various interactioncomponents that need to be considered to predict the structure and binding energetics of two compounds within activesite. In this case, the UDP-N-acetylmuramate-L-alanine ligase (**murC**) (PDB code: 1GQQ) with isocoumarin **4a**.

Figure 4 Complexity of protein–ligand interactions. The figure shows a schematic illustration of various interactioncomponents that need to be considered to predict the structure and binding energetics of two compounds within activesite. In this case, the UDP-N-acetylmuramate-L-alanine ligase (**murC**) (PDB code: 1GQQ) with isocoumarin **4b**.

Figure 5 Complexity of protein–ligand interactions. The figure shows a schematic illustration of various interactioncomponents that need to be considered to predict the structure and binding energetics of two compounds within activesite. In this case, the UDP-N-acetylmuramate-L-alanine ligase (**murC**) (PDB code: 1GQQ) with isocoumarin **4c**.

Figure 6 Complexity of protein–ligand interactions. The figure shows a schematic illustration of various interactioncomponents that need to be considered to predict the structure and binding energetics of two compounds within activesite. In this case, the UDP-N-acetylmuramate-L-alanine ligase (**murC**) (PDB code: 1GQQ) with isocoumarin **4d**.

Figure 7 Complexity of protein–ligand interactions. The figure shows a schematic illustration of various interactioncomponents that need to be considered to predict the structure and binding energetics of two compounds within activesite. In this case, the UDP-N-acetylmuramate-L-alanine ligase (**murC**) (PDB code: 1GQQ) with isocoumarin **4e**.

Figure 8 Complexity of protein–ligand interactions. The figure shows a schematic illustration of various interactioncomponents that need to be considered to predict the structure and binding energetics of two compounds within activesite. In this case, the UDP-N-acetylmuramate-L-alanine ligase (**murC**) (PDB code: 1GQQ) with isocoumarin **4f**.

Figure 9 Complexity of protein–ligand interactions. The figure shows a schematic illustration of various interactioncomponents that need to be considered to predict the structure and binding energetics of two compounds within activesite. In this case, the UDP-N-acetylmuramate-L-alanine ligase (**murC**) (PDB code: 1GQQ) with isocoumarin **4g**.

Table 1 Antibacterial activity results of isocoumarins **(4a-g)**

Table 2 AutoGrid Calculation around 8043 receptor atoms of UDP-N-acetylmuramate-L-alanine ligase with minimum and maximum interacting energies

Table 3 Calculation of Root Mean Square Deviation (RMSD) using the AutoDock Vina option of PyRx tool (Total runs=9)

Table 4 Interacting Energy obtained during docking of the compounds **(4a-g)** (Total runs=10)

Scheme 1 Synthesis of 3-alkyl/aryl substituted isocoumarins **(4a-g)**

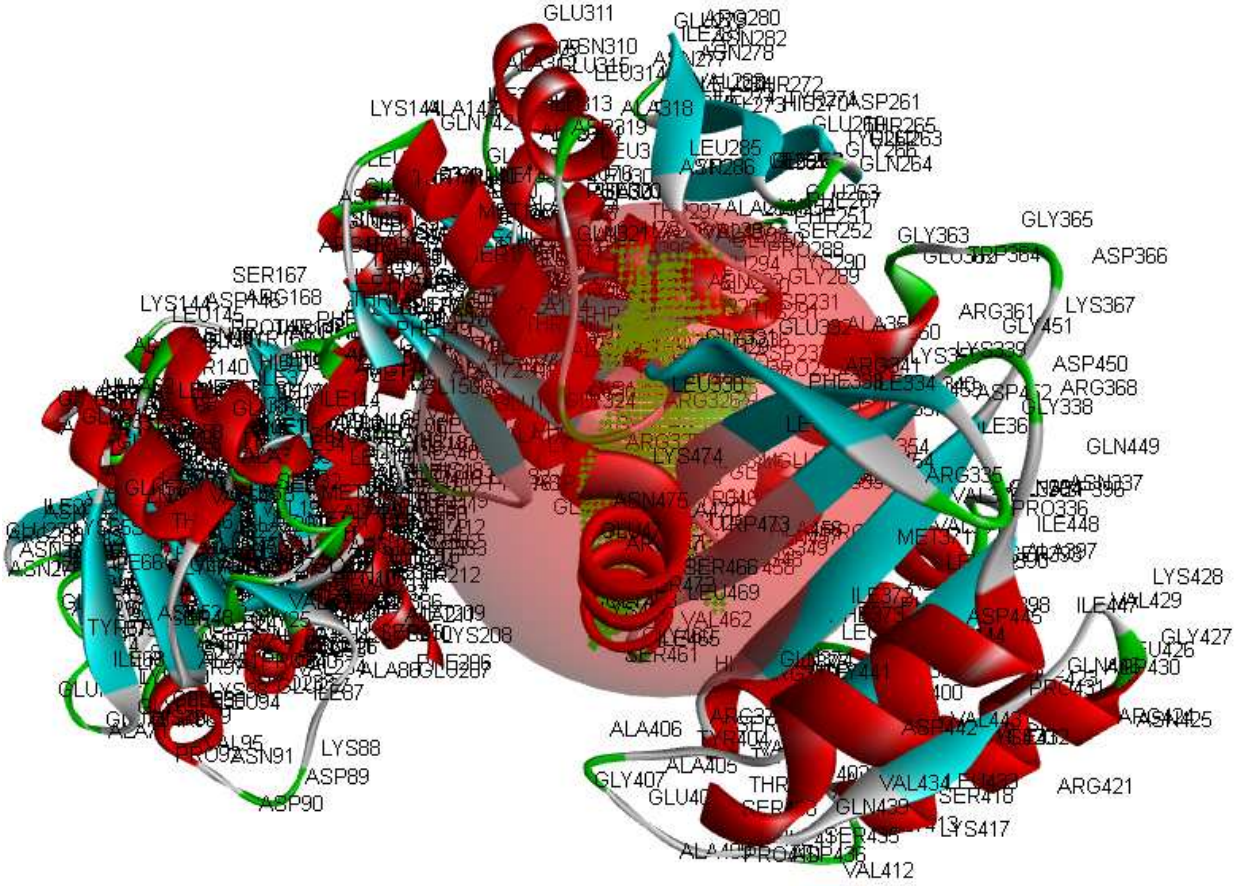

Figure 1 Amino acid residues on UDP-N-acetylmuramate-L-alanine ligase with shaded receptor binidng cavity defined by using Discovery Studio 3.0 Visualizer (PDB ID: 1GQQ)

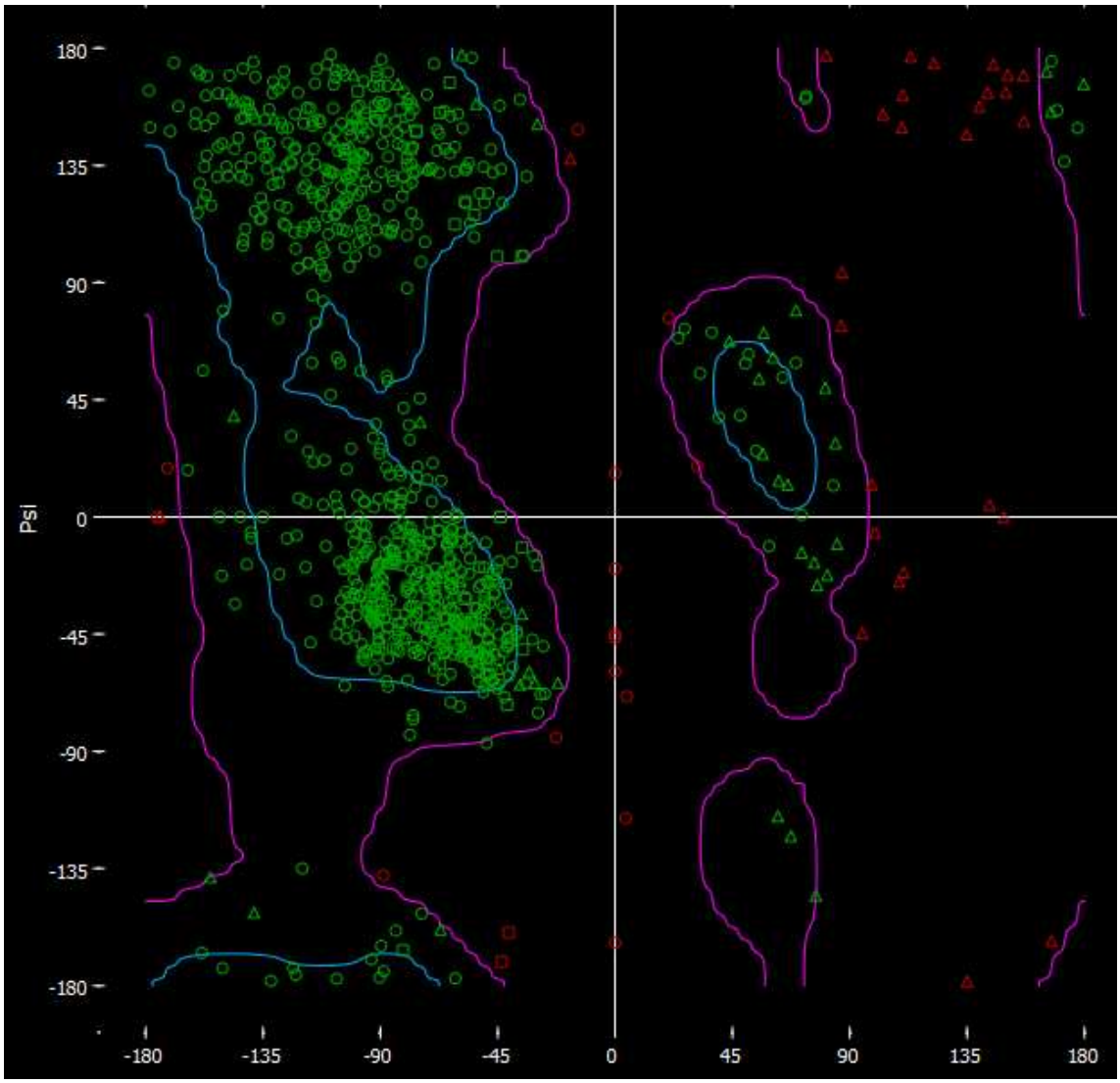

Figure 2 The Ramachandran Plot indicates low energy conformations for φ (phi) and ψ (psi), providing the graphical representation of the local backbone conformation of each residue of our target protein. Points on Plot are representing the φ and ψ torsion angles of a residue. It is also representing the favorable and unfavorable regions for residues.

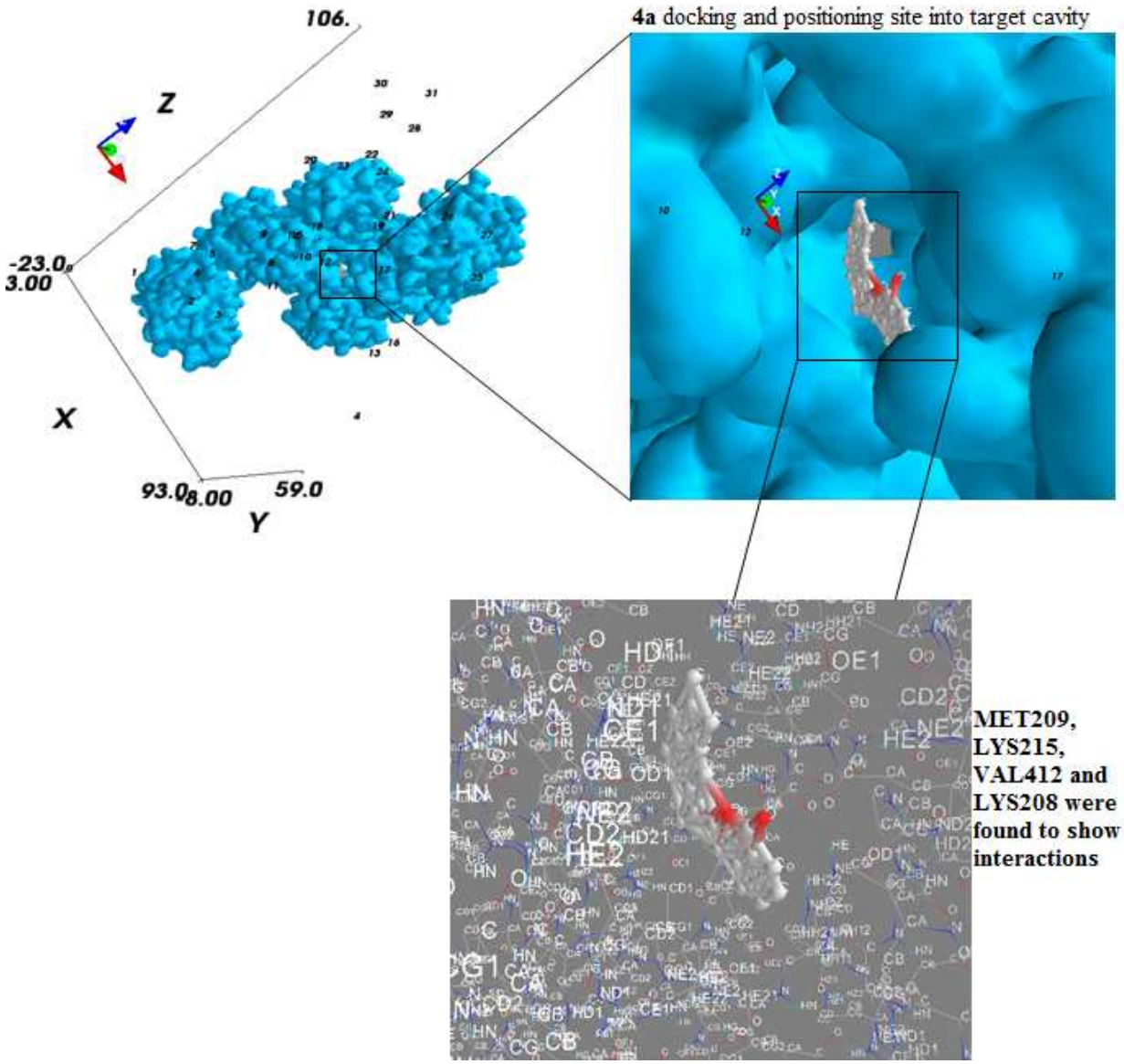

Figure 3 Complexity of protein-ligand interactions. The figure shows a schematic illustration of various interactioncomponents that need to be considered to predict the structure and binding energetics of two compounds within activesite. In this case, the UDP-N-acetylmuramate-L-alanine ligase (**murC**) (PDB code: 1GQQ) with isocoumarin **4a**.

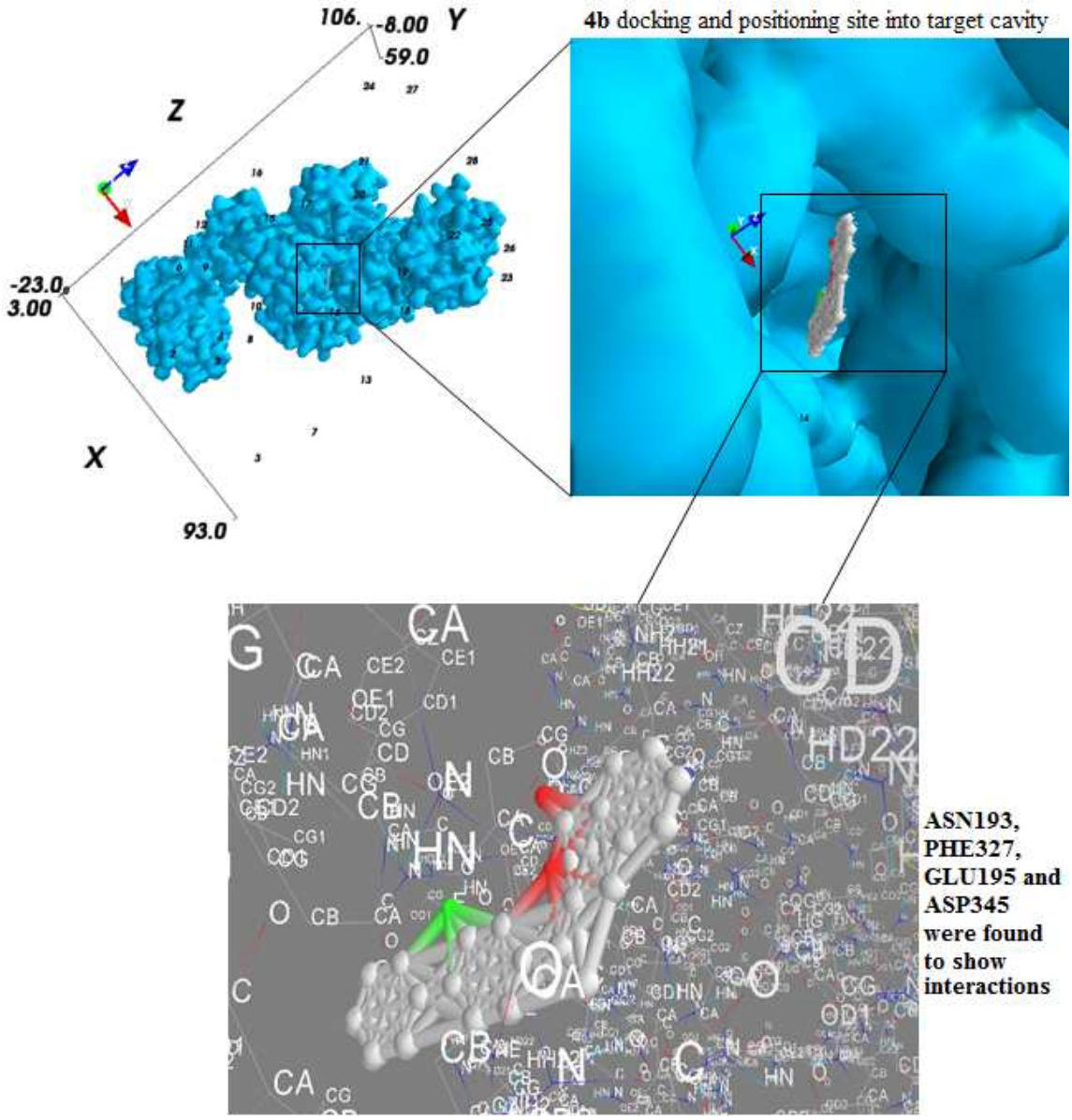

Figure 4 Complexity of protein-ligand interactions. The figure shows a schematic illustration of various interactioncomponents that need to be considered to predict the structure and binding energetics of two compounds within activesite. In this case, the UDP-N-acetylmuramate-L-alanine ligase (**murC**) (PDB code: 1GQQ) with **4b**.

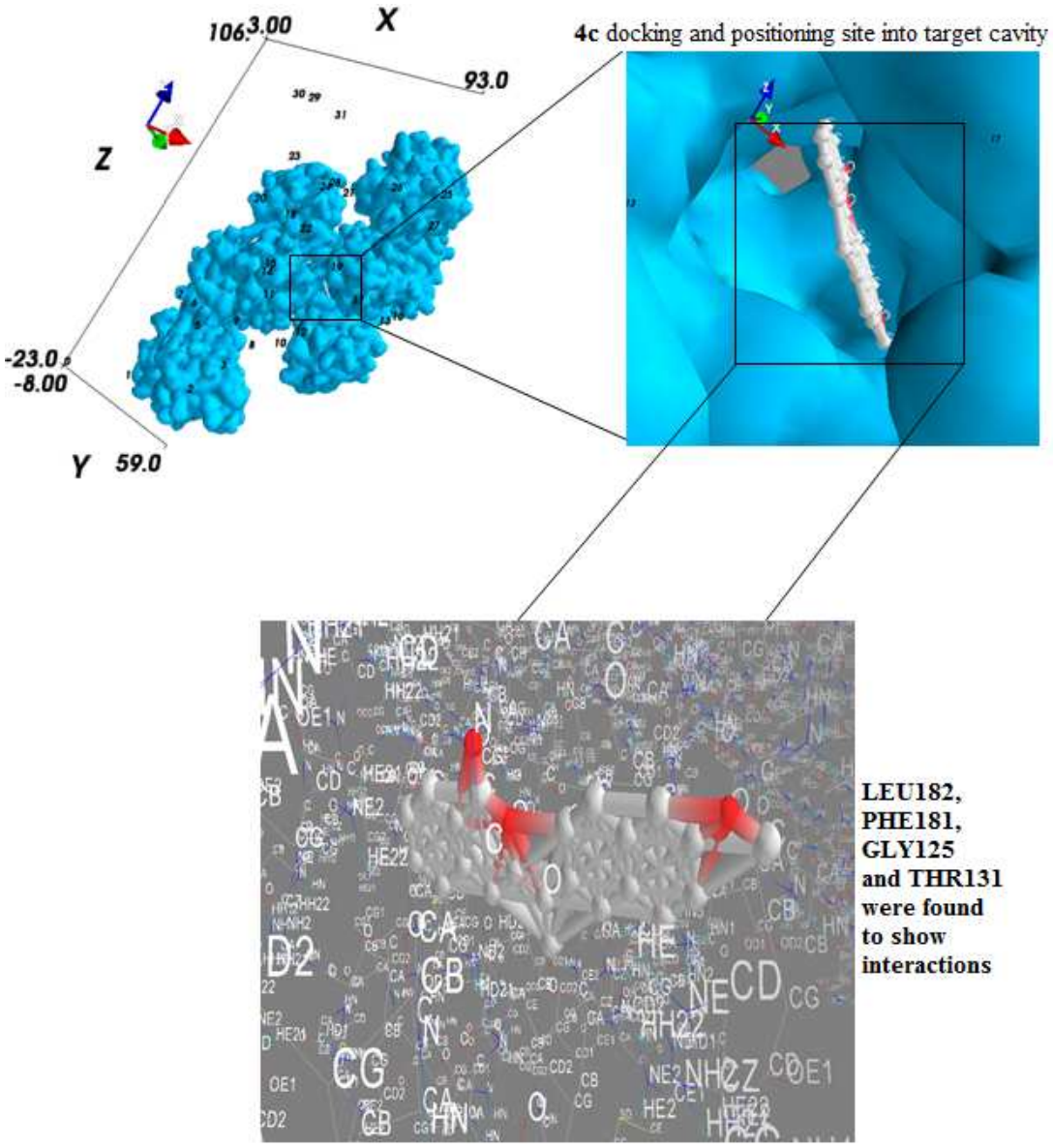

Figure 5 Complexity of protein-ligand interactions. The figure shows a schematic illustration of various interactioncomponents that need to be considered to predict the structure and binding energetics of two compounds within activesite. In this case, the UDP-N-acetylmuramate-L-alanine ligase (**murC**) (PDB code: 1GQQ) with **4c**.

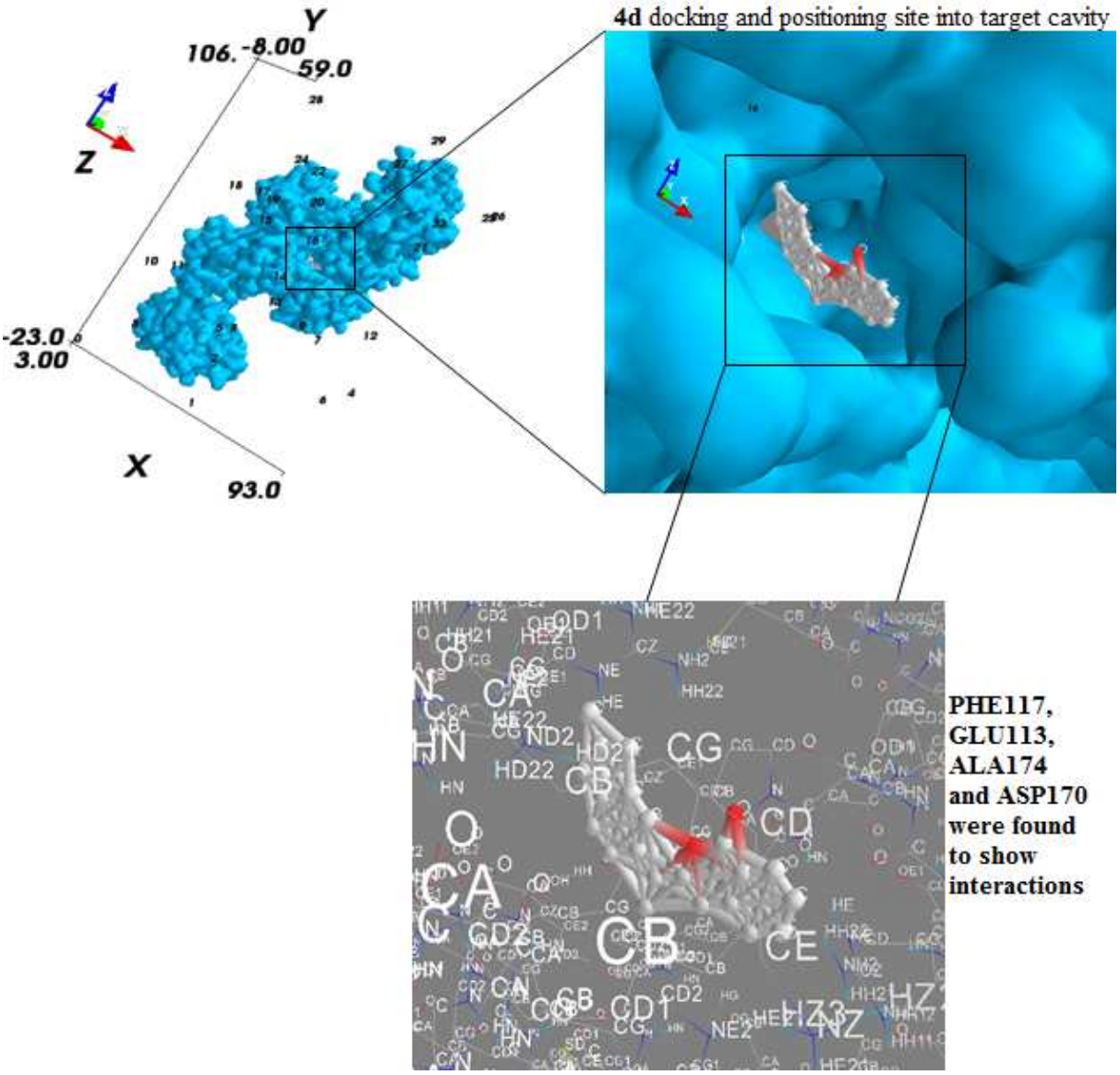

Figure 6 Complexity of protein–ligand interactions. The figure shows a schematic illustration of various interactioncomponents that need to be considered to predict the structure and binding energetics of two compounds within activesite. In this case, the UDP-N-acetylmuramate-L-alanine ligase (**murC**) (PDB code: 1GQQ) with **4d**.

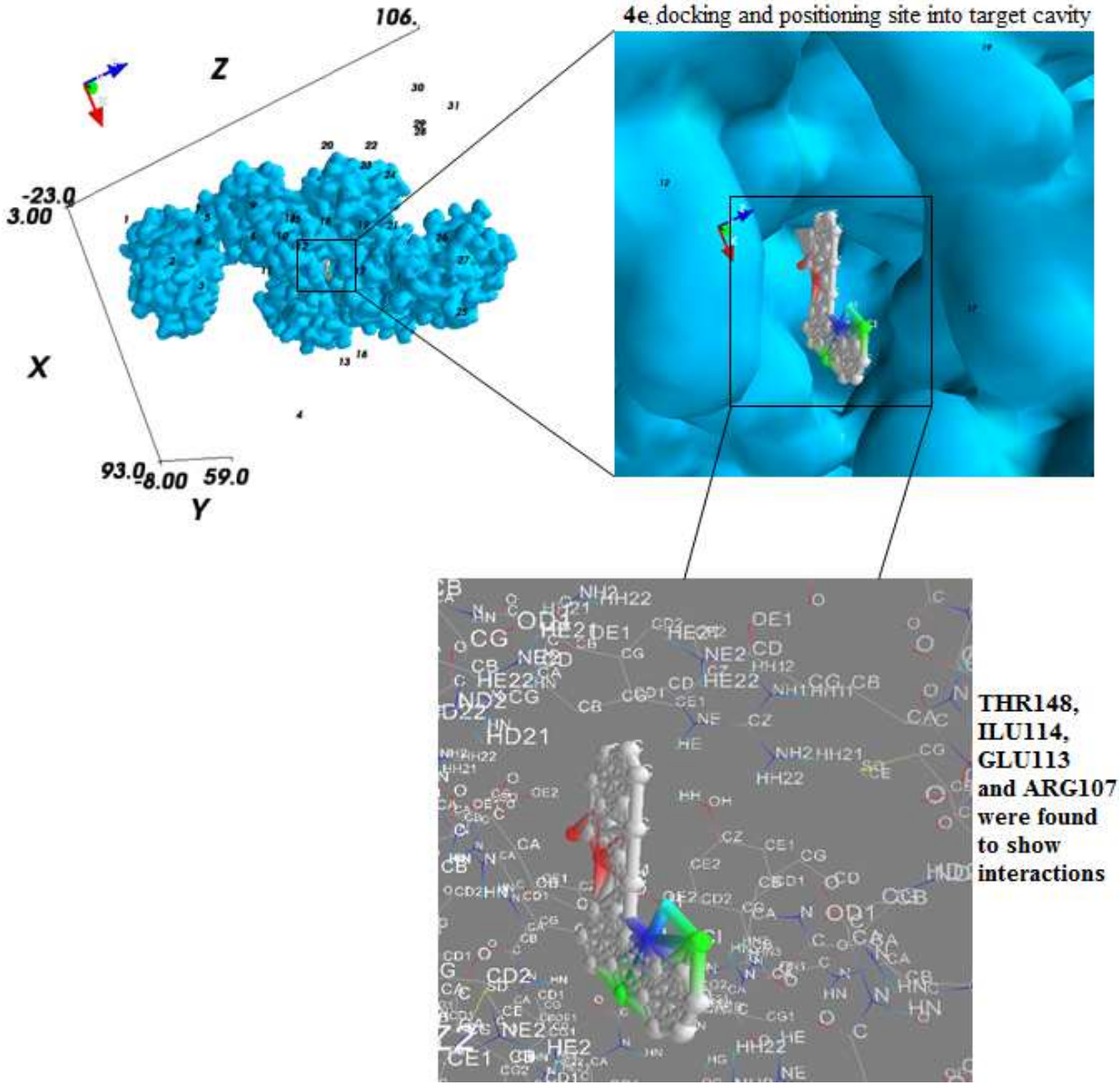

Figure 7 Complexity of protein-ligand interactions. The figure shows a schematic illustration of various interactioncomponents that need to be considered to predict the structure and binding energetics of two compounds within activesite. In this case, the UDP-N-acetylmuramate-L-alanine ligase (**murC**) (PDB code: 1GQQ) with **4e**.

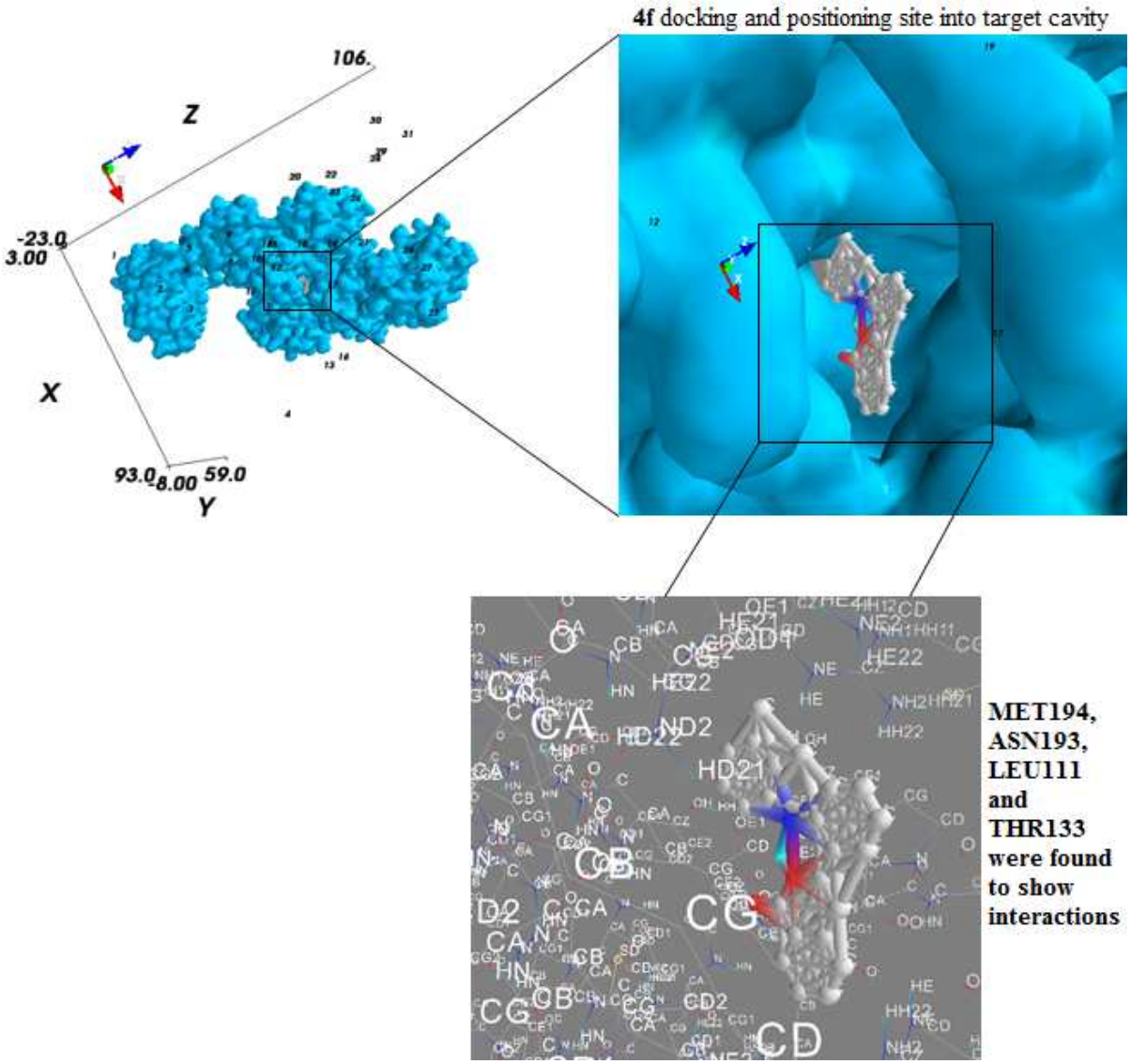

Figure 8 Complexity of protein-ligand interactions. The figure shows a schematic illustration of various interactioncomponents that need to be considered to predict the structure and binding energetics of two compounds within activesite. In this case, the UDP-N-acetylmuramate-L-alanine ligase (**murC**) (PDB code: 1GQQ) with **4f**.

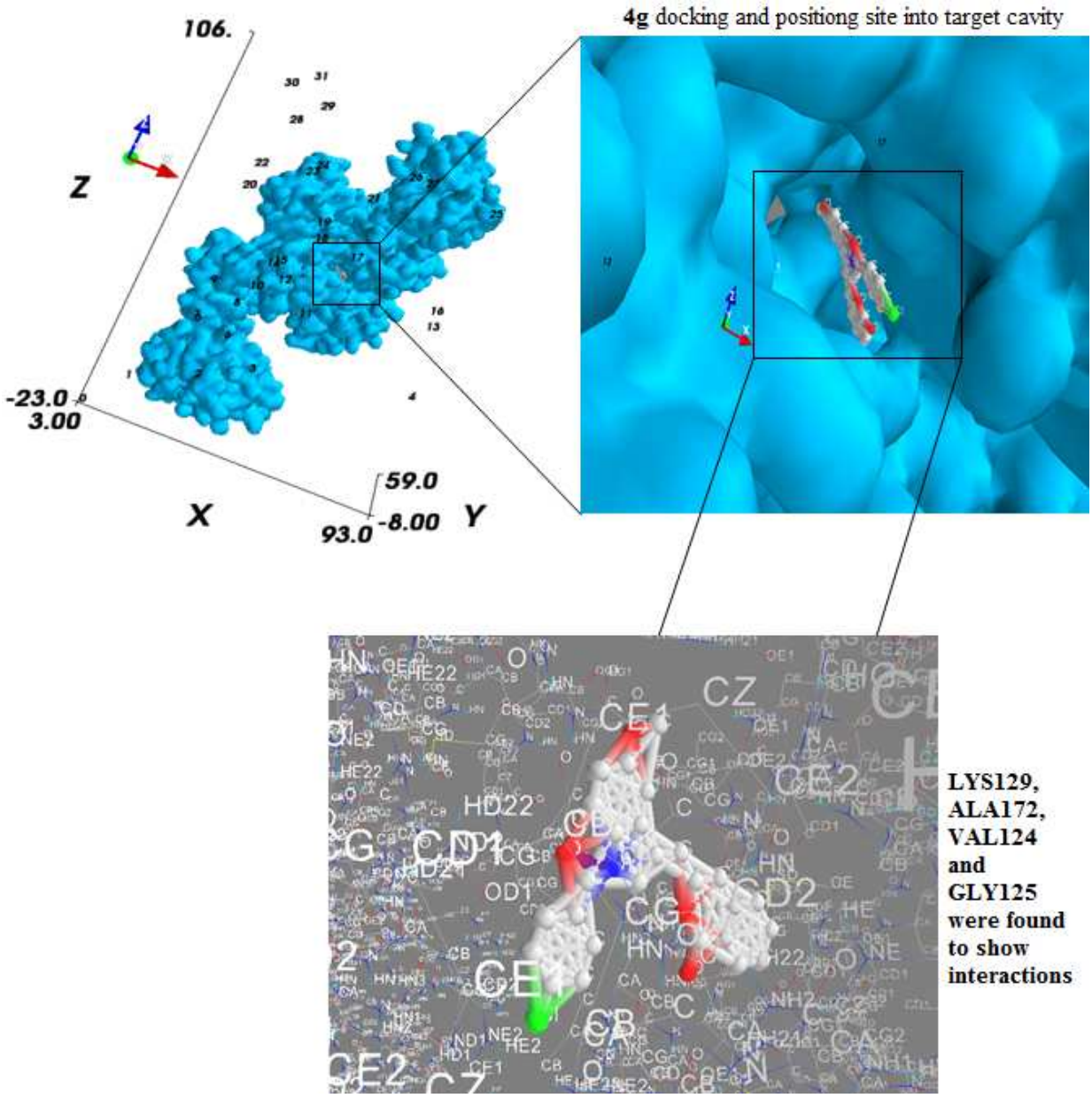

Figure 9 Complexity of protein-ligand interactions. The figure shows a schematic illustration of various interaction components that need to be considered to predict the structure and binding energetics of two compounds within activesite. In this case, the UDP-N-acetylmuramate-L-alanine ligase (**murC**) (PDB code: 1GQQ) with **4g**.

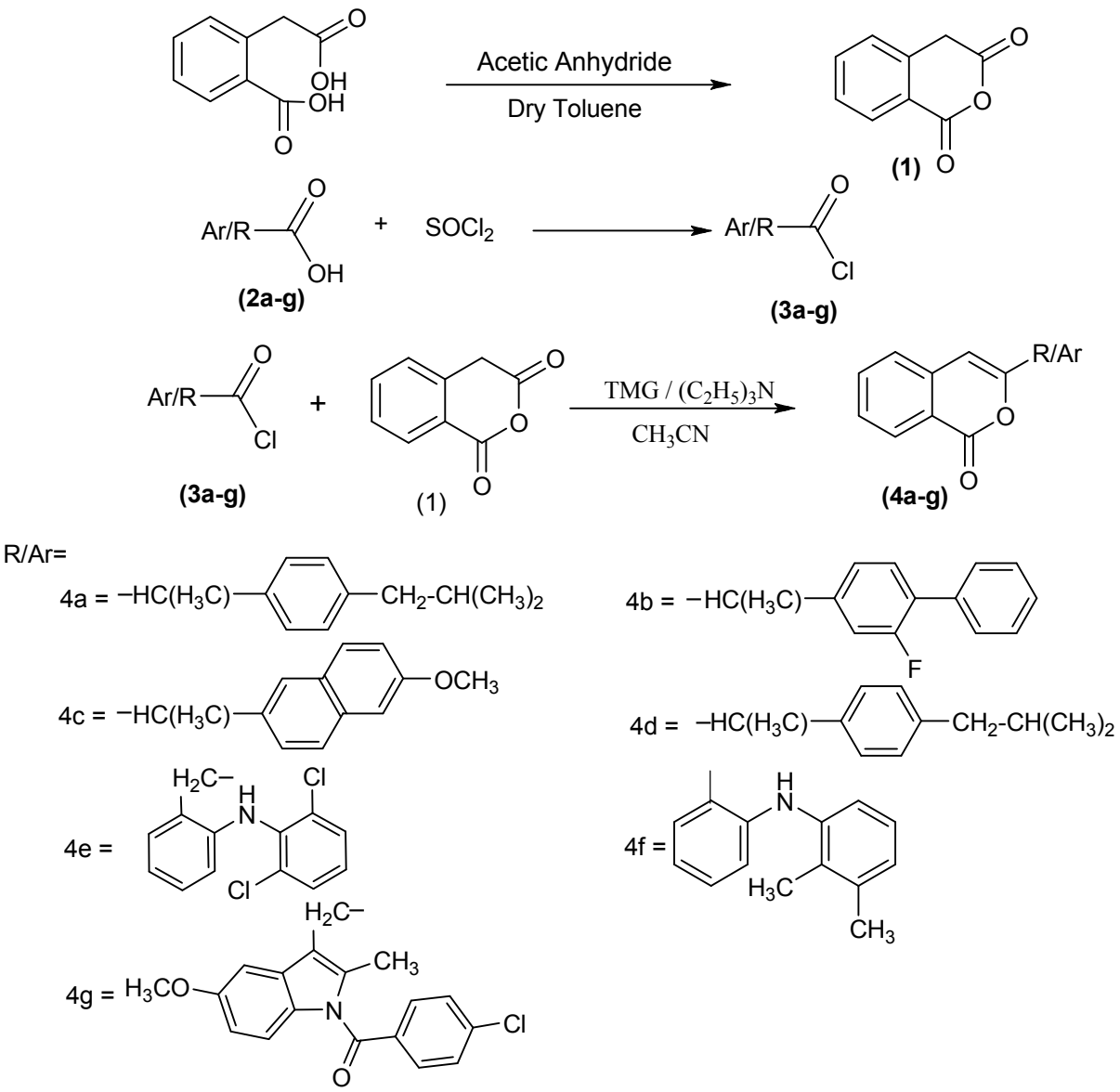

Scheme 1 Synthesis of 3-alkyl/aryl substituted isocoumarins **(4a-g)**

Table 1 Antibacterial activity results of isocoumarins (4a-g)

Codes	***P.m.***	***B.s.***	***E.c.***	***S.a.***	***P.p.***	***P.a.***	***S.t.***	***M.l.***	***S. f.***	***K.p.***
4a	23	11	20	15	19	16	19	20	14	17
4b	10	08	13	07	-	-	-	04	-	02
4c	24	-	26	-	26	19	25	-	24	17
4d	-	-	-	11	-	-	-	07	05	-
4e	06	05	11	-	-	07	10	12	13	06
4f	24	16	18	17	23	21	25	19	26	20
4g	26	18	19	20	26	20	24	16	19	22
Standard	30	20	30	25	30	28	30	25	30	25

Activity is presented in millimeter (mm), **(-)** No activity

Proteus mirabilis ***(P.m.)***, *Bacillus subtilis* ***(B.s.)***, *Escherichia coli* ***(E.c.)***, *Staphylococcus aureus* ***(S.a.)***, *Pseudomonas putida* ***(P p.)***, *Pseudomonas aeruginosa* ***(P.a.)***, *Salmonella typhi* ***(S.t.)***, *Micrococcus luteus* ***(M.l.)***, *Shigella flexineri* ***(S.f.)*** and *Klebsiella pneumonae* ***(K.p.)***.

Table 2 AutoGrid Calculation around 8043 receptor atoms of UDP-N-acetylmuramate-L-alanine ligase with minimum and maximum interacting energies

Ligand Codes	Grid Map	Atom Type	Minimum Energy (kcal/mol)	Maximum Energy (kcal/mol)	Setting parameters in PyRx
4c	1	A	-0.88	2.03e+05	-
	2	OA	-1.78	2.00e+05	-
	3	e	-32.71	3.33e+01	Electrostatic Potential
	4	d	0.00	1.45e+00	Desolvation Potential
4b	1	A	-0.88	2.03e+05	-
	2	OA	-1.78	2.00e+05	-
	3	F	-0.66	2.00e+05	-
	4	e	-32.71	3.33e+01	Electrostatic Potential
	5	d	0.00	1.45e+00	Desolvation Potential
4g	1	A	-0.88	2.03e+05	
	2	Cl	-1.29	2.04e+05	
	3	OA	-1.78	2.00e+05	
	4	N	-1.04	2.01e+05	
	5	e	-32.71	3.33e+01	Electrostatic Potential
	6	d	0.00	1.45e+00	Desolvation Potential
4f	1	A	-0.88	2.03e+05	
	2	HD	-0.72	1.13e+05	
	3	OA	-1.78	2.00e+05	
	4	N	-1.04	2.01e+05	
	5	e	-32.71	3.33e+01	Electrostatic Potential
	6	d	0.00	1.45e+00	Desolvation Potential
4e	1	A	-0.88	2.03e+05	
	2	Cl	-1.29	2.04e+05	
	3	HD	-0.72	1.13e+05	
	4	OA	-1.78	2.00e+05	
	5	N	-1.04	2.01e+05	
	6	e	-32.71	3.33e+01	Electrostatic Potential
	7	d	0.00	1.45e+00	Desolvation Potential
4a	1	A	-0.88	2.03e+05	
	2	OA	-1.78	2.00e+05	
	3	e	-32.71	3.33e+01	Electrostatic Potential
	4	d	0.00	1.45e+00	Desolvation Potential
4d	1	A	-0.88	2.03e+05	
	2	OA	-1.78	2.00e+05	
	3	e	-32.71	3.33e+01	Electrostatic Potential
	4	d	0.00	1.45e+00	Desolvation Potential

Table 3 Calculation of Root Mean Square Deviation (RMSD) using the AutoDock Vina option of PyRx tool (Total runs=9)

Ligand Code	Ligand-Target complex	Binding Affinity	RMSD/ub	RMSD/ub
4a	1GQQ_4a	-11.9	4.273	0.668
4b	1GQQ_4b	-12.7	4.948	1.309
4c	1GQQ_4c	-12	3.456	2.834
4d	1GQQ_4d	-5.1	1.081	0.814
4e	1GQQ_4e	-13.1	4.789	1.716
4f	1GQQ_4f	-12.9	4.698	1.36
4g	1GQQ_4g	-13.8	4.772	1.98

Table 4 Interacting Energy obtained during docking of the compounds **4a-g** (Total runs=10)

Ligand Code	Ligand-Target complex	Binding Energy	Intermol Energy	Internal Energy	Torsional Energy	Unbound Energy
4a	1GQQ_4a	-10.33	-10.92	0	0.6	0
4b	1GQQ_4b	-10.52	-11.42	0	0.89	0
4c	1GQQ_4c	-10.05	-10.95	0	0.89	0
4d	1GQQ_4d	-10.31	-10.91	0	0.6	0
4e	1GQQ_4e	-11.09	-11.99	0	0.89	0
4f	1GQQ_4f	-10.63	-11.53	0	0.89	0
4g	1GQQ_4g	-12.26	-13.75	0	1.49	0